Journal of Biomedical Optics

SPIEDigitalLibrary.org/jbo

Parallel acoustic delay lines for photoacoustic tomography

Murat Kaya Yapici
Chulhong Kim
Cheng-Chung Chang
Mansik Jeon
Zijian Guo
Xin Cai
Jun Zou
Lihong V. Wang

SPIE

Parallel acoustic delay lines for photoacoustic tomography

Murat Kaya Yapici,[a*] Chulhong Kim,[b*] Cheng-Chung Chang,[c] Mansik Jeon,[b] Zijian Guo,[d] Xin Cai,[d] Jun Zou,[c] and Lihong V. Wang[d]
[a]Khalifa University, Department of Electrical and Computer Engineering, Abu Dhabi, UAE
[b]The State University of New York, The University at Buffalo, Department of Biomedical Engineering, Buffalo, New York 14260
[c]Texas A&M University, Department of Electrical and Computer Engineering, College Station, Texas 77843
[d]Washington University in St. Louis, Department of Biomedical Engineering, St. Louis, Missouri 63130

Abstract. Achieving real-time photoacoustic (PA) tomography typically requires multi-element ultrasound transducer arrays and their associated multiple data acquisition (DAQ) electronics to receive PA waves simultaneously. We report the first demonstration of a photoacoustic tomography (PAT) system using optical fiber-based parallel acoustic delay lines (PADLs). By employing PADLs to introduce specific time delays, the PA signals (on the order of a few micro seconds) can be forced to arrive at the ultrasonic transducers at different times. As a result, time-delayed PA signals in multiple channels can be ultimately received and processed in a serial manner with a single-element transducer, followed by single-channel DAQ electronics. Our results show that an optically absorbing target in an optically scattering medium can be photoacoustically imaged using the newly developed PADL-based PAT system. Potentially, this approach could be adopted to significantly reduce the complexity and cost of ultrasonic array receiver systems. [DOI: 10.1117/1.JBO.17.11.116019]

Keywords: photoacoustic tomography; acoustic delay line: ultrasound transducer array: real-time imaging.

Paper 12393 received Jun. 26, 2012; revised manuscript received Sep. 25, 2012; accepted for publication Oct. 1, 2012; published online Nov. 7, 2012.

1 Introduction

Photoacoustic tomography (PAT) has emerged as a hybrid biomedical imaging technique which combines strong endogenous and exogenous optical absorption contrast and high ultrasonic resolution in a single modality.[1–3] In PAT, a short-pulsed laser irradiates the biological tissue, and photoacoustic (PA) waves are generated via thermoelastic expansion. These PA waves propagate in the medium and are then detected by a single-element ultrasonic transducer or an ultrasonic transducer array. The amplitudes of the initial PA waves, the multiplication between local fluence, and the optical absorption coefficients of targets represent the optical absorption distribution of the tissue. Thus, PAT overcomes the fundamental limitations of pure optical imaging (shallow imaging depth for high resolution, or poor spatial resolution beyond the transport mean free path) and pure ultrasonic imaging (weak contrast for detecting early stage cancers and speckle artifacts).[4–9] It is capable of high-resolution structural,[10,11] functional,[11–14] and molecular imaging.[15–20] By scaling the ultrasonic frequency, the spatial resolution and imaging depth can be tailored for particular imaging applications.

There are two main types of PAT systems.[21] The first is photoacoustic microscopy (PAM), which utilizes direct point-by-point detection of 1-D depth-resolved images and raster mechanical scanning to form a 3-D image. The second type is photoacoustic computed tomography (PACT), which uses ultrasonic transducer arrays for parallel detection and reconstruction algorithms for real-time image generation.[22–25] PAM does not require the use of a mathematical algorithm to generate an image, but it requires raster scanning with a single-element focused transducer. Consequently, the imaging speed of PAM depends largely on the laser repetition rate and the speed of the mechanical scanning. By contrast, PACT can be implemented using an ultrasound array system; hence, the imaging speed is dramatically improved without raster mechanical scanning. For example, Gamelin et al.[23] used a full-ring ultrasonic transducer array consisting of 512 elements to collect two-dimensional (2-D) images at a frame rate of 0.9 Hz, with a 10-Hz laser pulse repetition rate. The data acquisition (DAQ) electronics were composed of 512 low-noise preamplifiers. With 8:1 multiplexing, eight laser pulses were required to capture a complete 512-element data set. In addition, linear ultrasound transducer arrays with either 48 or 128 elements have been used in PACT.[23,25]

Generally, the imaging speed of PACT depends on the number of transducer elements in the array. However, as the number of transducer elements increases, the construction and operation of the ultrasound receiving systems becomes more challenging and costly. Therefore, new solutions are needed to reduce or even completely eliminate the dependence on massive ultrasonic transducer arrays and extensive DAQ electronics.

Depending on the penetration depth (from a few mm to cm) and the acoustic velocity in the target tissue (~1480 m/s), the typical propagation time of a PA wave in the tissue medium is on the order of microseconds (μs) [Fig. 1(a)]. On the other hand, the pulse repetition rate of the pulsed-laser systems used in PAT is in the kilohertz range, so the time interval between two successively generated PA waves will be on the order of milliseconds (ms). In current PACT systems, all the generated PA signals propagate and reach the ultrasonic transducers nearly simultaneously. This simultaneity inevitably leads to a parallel detection scheme, which requires multiple receiving channels (including ultrasonic transducers and DAQ electronics). However, by using parallel acoustic delay lines (PADLs) to introduce

*These authors contributed equally to this work.

Address all correspondence to: Lihong V. Wang, Washington University in St. Louis, Department of Biomedical Engineering, St. Louis, Missouri 63130. Tel: 314-935-6152; Fax: 314-935-7448; E-mail: lhwang@biomed.wustl.edu

0091-3286/2012/$25.00 © 2012 SPIE

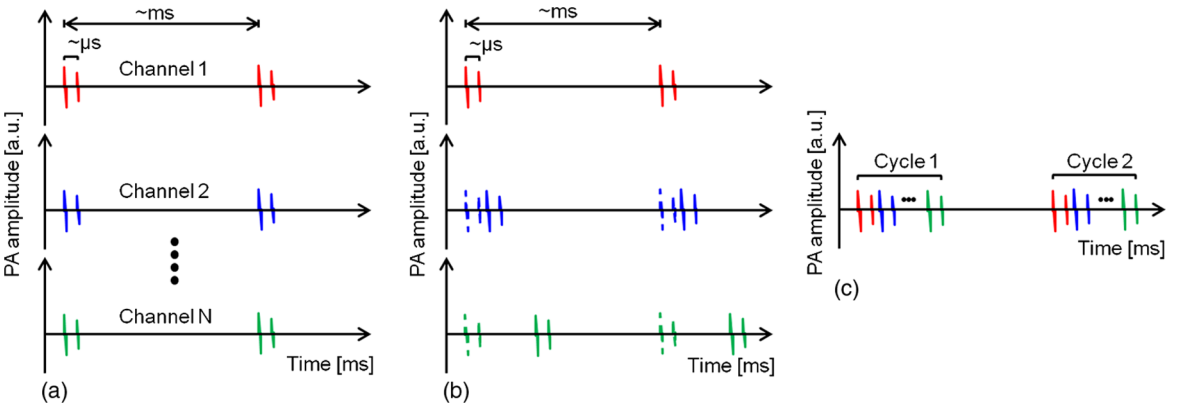

Fig. 1 (a) PA signals without time delays (in current PACT systems); (b) PA signals with proper time delays; and (c) multiple channels of time-delayed PA signals mixed into one single channel.

specific acoustic time delays [Fig. 1(b)], the PA signals in different channels can be forced to arrive at the ultrasonic transducers at different times, and will be completely distinguishable in the time domain even after being mixed into one channel [Fig. 1(c)]. Ultimately, this technique opens the possibility of detecting and processing multiple channels of time-delayed PA signals in a serial manner, using a single-element transducer and single-channel DAQ electronics. Because the PA signals have a shorter propagation time (μs) than the laser pulse repetition time (ms), this approach is potentially able to merge a large number of receiving channels, and thus leads to significant reductions in the complexity and cost of ultrasonic receiving systems.

In this paper, we report, for the first time to our knowledge, the development and application of a novel PADL technique for PAT. The PADLs are made of low-loss and flexible optical fibers. We experimentally characterized the acoustic properties of the optical fibers and verified the feasibility of using them as acoustic waveguides. Based on these results, the optical fibers were used to construct multi-channel PADLs where each channel independently carried PA waves with a specific time delay. We built a prototype PADL-PAT system using 16 optical-fiber PADLs, 2 ultrasound transducers, and 2 channels of DAQ electronics. The PADL-PAT system successfully imaged an optically absorbing object positioned in an optically scattering medium.

2 Optical-Fiber Acoustic Waveguides

Various materials, including liquid mercury,[26] solid quartz crystals,[27] metallic wires,[28] and flexible optical fibers,[29,30] have been used to construct ultrasonic delay lines. Given the acoustic velocity in these media, we can control the acoustic time delay from μs to ms by varying the propagation length of the material without causing excessive acoustic attenuation.[31] To construct the delay line for this work, we selected optical fibers due their broad availability, low cost, and low acoustic attenuation.

2.1 *Propagation Modes in Optical Fibers*

PA signals propagate in longitudinal modes. However, for wire-type cylindrical acoustic delay lines, all of the sustained longitudinal modes are dispersive, which means that the time delay is dependent on the frequency of the transmitted signal. This dispersion can generate signal distortion in the time domain, which is not desirable for PAT since the time-of-arrival of the PA signals is used to retrieve spatial information for image reconstruction. To address this issue, the lowest-order longitudinal mode [$L(0,1)$] of the Pochhammer-Chree wave was used. It has been shown that if the diameter of the circular fiber (d) is much smaller than the ultrasound wavelength (λ) both the higher-order longitudinal modes and the dispersion of the $L(0,1)$ mode will be significantly suppressed. Typically, this condition is satisfied when (d/λ) or (df/V_0) <0.1, where f is the frequency of the ultrasonic wave, and V_0 is the acoustic velocity in a rod.[28,32] A smaller ratio of (df/V_0) would further suppress higher order modes and the dispersion of the $L(0,1)$ mode. Thus, once d is small enough that the above inequality is satisfied for all detected wave components, high-fidelity transmission of the PA signal through the acoustic delay lines can be achieved. However, if d is too small, it would be difficult to transmit sufficient PA signals via the fiber, and thus the PAT system would suffer from low signal-to-noise ratio (SNR) because of the narrow detector area. For PA signal detection at a 1 MHz center frequency, and based on previously reported acoustic velocity data for optical fibers (5000 to 6000 m/s),[32,33] fibers with a total diameter of ~245 μm were selected for this work, which provided (df/V_0) <0.05. The silica-silica (all-silica) optical fibers used in this work have a pure silica core with 200 μm diameter, surrounded by a 20-μm-thick cladding layer made of fluorine doped silica, and an outer 25-μm-thick polyimide jacket layer (Optran WF 200/220*P* from Ceram-Optec Industries Inc., MA).

2.2 *Characterization Method*

To build an optical fiber-based delay line, the acoustic properties (i.e., attenuation, propagation velocity, and time delay) of silica optical fibers were characterized. The schematic and a photograph of the experimental setup are shown in Fig. 2. The optical fiber was loosely mounted onto a phenolic-based (acrylic) perforated board (proto-board) and the unnecessary contact between the fiber and surrounding structures was minimized to reduce acoustic reverberation. Two identical flat, longitudinal mode PZT ultrasound transducers with a center frequency of 1 MHz (Olympus NDT, V303) were used. The fiber tips were polished and carefully coupled to the transducer surface via a thin layer of ultrasound gel. This coupling also helped to filter out the unwanted shear, torsional, and extensional modes of the ultrasonic waves. Optical fibers with various lengths were tested for acoustic attenuation, ultrasound propagation velocity, and time delay. As shown in Fig. 2(b), an ultrasound pulse (1 μs width and 500 mV amplitude) was generated by a signal generator, amplified by an RF amplifier, and applied to the transmitting transducer. Ultrasound pulses from the transmitting

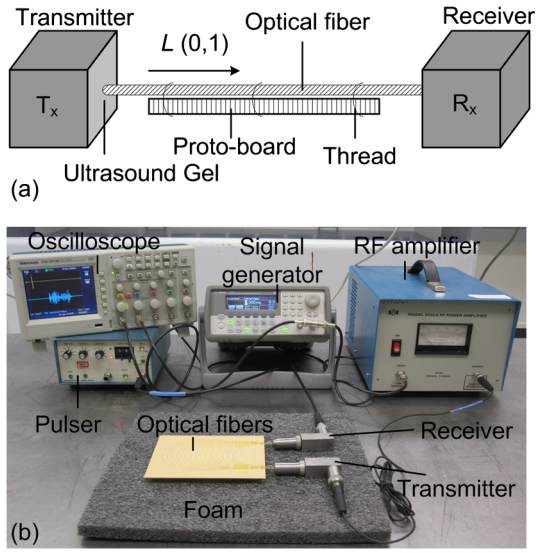

Fig. 2 (a) Schematic showing the arrangement of transducers with respect to the optical fiber under characterization; and (b) photograph of the entire experimental setup for acoustic characterization of optical fibers.

transducer propagated through the optical fiber and were detected by the receiving transducer. The received signals were amplified and displayed on an oscilloscope.

2.3 *Acoustic Properties: Attenuation, Velocity, and Time Delay*

Figure 3(a) shows the detected ultrasound waveforms for six optical fibers of varying lengths, as well as the ultrasound pulse applied to the transmitting transducer. Distinct signals at an incremental time delay of ~10 μs were received for fibers of lengths ranging from 10 to 35 cm. For shorter fibers, the 1st echo signals resulting from acoustic reflection between the fiber and the surface of the receiving transducer are also displayed. The echoes were detected at a time corresponding to three traversals of the fiber length. The time delay of each fiber is plotted in Fig. 3(b). As the fiber length increases, the time delay increases linearly. Based on these measurements, the average acoustic velocity in silica optical fiber was found to be ~5108 m/s.

To determine the acoustic attenuation in the optical fibers, the amplitudes of the received ultrasound waves were also plotted [Fig. 3(c)]. The amplitudes can be used to calculate the acoustic loss (L), which is defined by 20 $\log(V_{\text{out}}/V_{\text{in}})$, where V_{in} refers to the acoustic signal amplitude at the fiber input, and V_{out} refers to the amplitude at the output. The acoustic attenuation constant can then be calculated by dividing the acoustic loss by the length of the optical fiber. However, it is difficult to directly measure V_{in}. Therefore, losses of two different fibers (with Δl finite length difference) were subtracted. Then, the loss over Δl length is 20 $\log(V_{\text{out},i}/V_{\text{out},1})$, where $V_{\text{out},1}$ (the shorter fiber) was kept constant in all calculations, and $V_{\text{out},i}$ corresponds to the output amplitudes of the remaining five fibers ($i = 2$ to $i = 6$). Based on this approach, five data points for loss (i.e., $L_{2,1}$ to $L_{6,1}$) were obtained [inset in Fig. 3(c)], and the average attenuation per unit length or unit time delay was calculated as ~0.2 dB/cm (i.e., 0.1 dB/μs) at 1 MHz, which matches well with previously reported data.[32]

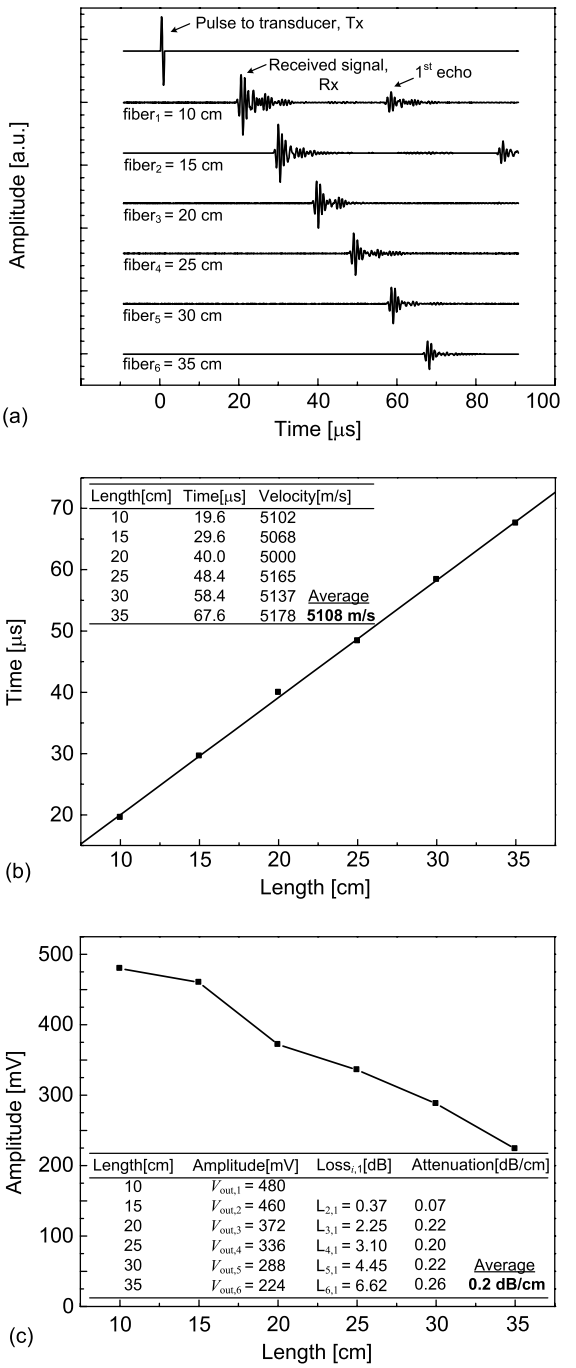

Fig. 3 (a) Plot showing acoustic waveforms propagating through optical fibers of different lengths ranging from 10 to 35 cm. (b) Plot of the time delay versus the corresponding fiber length. The average acoustic velocity in the silica fiber is ~5108 m/s. (c) Attenuation of acoustic signals through optical fibers of various lengths. The average attenuation is ~0.2 dB/cm (0.1 dB/μs).

To analyze the frequency response of the optical fibers, a fast Fourier transform (FFT) operation was performed on their time-domain response [ultrasound waveforms in Fig. 3(a)] using the built-in FFT algorithm of MATLAB®. Power spectra of the six different optical fibers are plotted on the same chart for comparison [Fig. 4(a)].

On average, the signals have a center frequency at ~1 MHz and −6 dB bandwidth of ~0.5 MHz, with upper and lower frequency cutoffs at ~0.85 and ~1.35 MHz, respectively. The

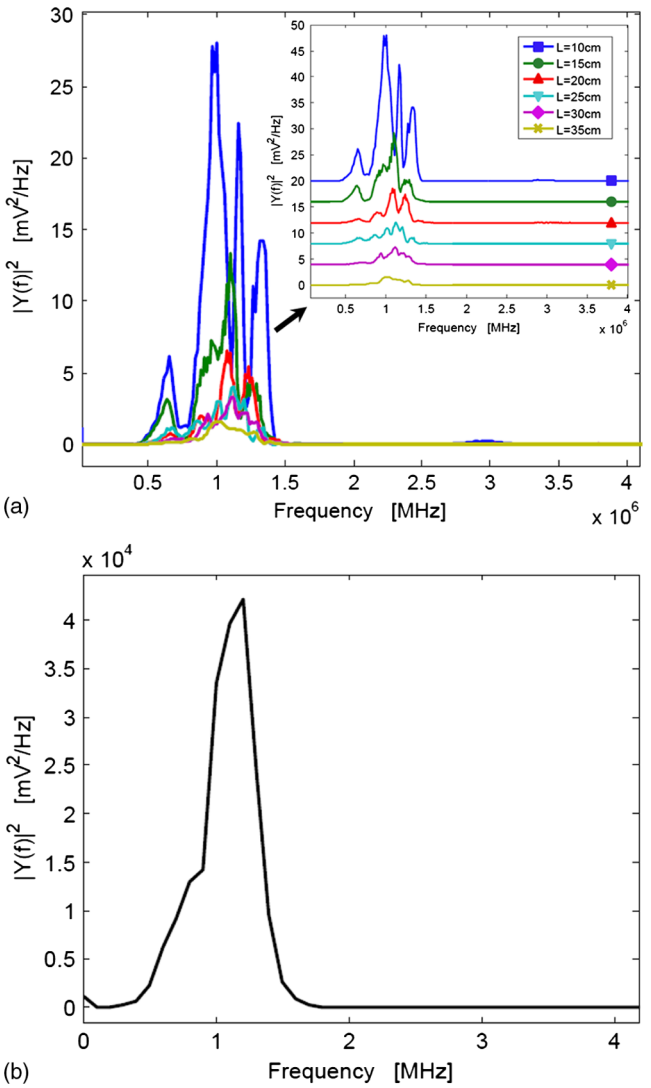

Fig. 4 (a) Frequency response (power spectra) of the six optical fibers with different lengths, showing a center frequency of ~1 MHz. Inset shows the spectra spaced-out in *y*-axis for visualization. (b) Frequency response of the transducer used in the experiments.

same approach was used to obtain the frequency response of the transducer [Fig. 4(b)]; where, the transmitting and receiving transducers are directly coupled to each other with no delay lines in between. The spectrum shows that the transducer center frequency of ~1 MHz is similar to datasheet specifications,[34] which also matches with the received power spectra of the fibers [Fig. 4(a)].

3 Parallel Acoustic Delay Lines

The optical-fiber PADLs were designed based on the measured acoustic properties of optical fibers. The following design parameters were also considered: (1) the number of fibers (i.e., the number of delay lines, n), (2) the length of each fiber (to determine the time delay), and (3) the parallel arrangement of fibers and the pitch between fibers. As n increases, the construction and handling of the PADLs becomes difficult due to the longer fiber lengths. In this work, n was selected as 8 to ensure a compact design and an adequate field-of-view (FOV), which is also related to the fiber diameter, pitch, and target size in PA imaging. When the fiber lengths were determined, the following two

Table 1 Time delays and optical fiber lengths for PADLs.

Fiber number	Signal arrival (μs)	1st Echo arrival (μs)	Fiber length (mm)
1	44	132	225
2	56	168	286
3	68	204	347
4	80	240	409
5	92	276	470
6	104	312	531
7	116	348	593
8	128	384	654

The incremental time delay between fibers is 12 μs, and the acoustic velocity in silica optical fibers is ~5108 m/s.

design criteria were considered. First, the time delay between each fiber (i.e., channel spacing) should be long enough to prevent possible signal overlaps from adjacent channels. Based on the duration (~12 μs) of the ultrasonic signals arriving at the receiving transducer, an incremental time delay (≥12 μs) between adjacent delay lines is required to avoid signal overlapping. The second criterion concerning fiber lengths is to select the proper arrival time for reflected signals (1st echo) in the shortest fiber (1st fiber). To prevent possible interference between echoes and the original signals propagating in neighboring fibers, the fiber with the longest time-delay (nth fiber) should be designed so that its signal reaches the receiving transducer before the 1st fiber's echo does. Denoting T as the incremental time delay between two neighboring fibers, and T_1 as the time delay of the 1st fiber, the signal in the nth fiber will be received at $T_1 + T(n-1)$, while the 1st fiber's echo will be received at $3T_1$. Then, to prevent interference, the following inequality must hold: $3T_1 > T_1 + T(n-1)$. Therefore, for an 8-fiber delay line and 12-μs incremental time delay, T_1 should be longer than 42 μs. Based on this result, the 1st and 8th fibers were designed to provide time delays of 44 and 224 μs, respectively, which creates a 4-μs gap between the arrival of the 1st fiber's echo and the signal in the 8th fiber. Table 1 summarizes the time delays (timing of signals and echoes) for the 8-channel optical-fiber PADL system, along with the corresponding fiber lengths.

In ultrasound array systems, it is common to arrange the transducer elements with $p < \lambda/2$, where p is the pitch and λ is the wavelength. Based on the frequency (1 MHz) of our ultrasound transducers, the fiber-to-fiber spacing would be in the range of 400 to 500 μm. To arrange the optical-fiber PADLs, ~200-μm-wide trenches in parallel (pitch ~450 μm) were made in a low-loss acoustic material (lucite) [Fig. 5(a)]. The fibers were loosely placed in trenches, which allowed for side-by-side arrangement of fiber endings at the input and output ports with the correct pitch and minimal attenuation. A total of sixteen fibers are housed in a common input port for PA signal detection, and separated into two output ports for time-delayed read-out [Fig. 5(c)]. The selected geometrical dimensions, including the fiber diameter and spacing, as well as the number of fibers provide an effective FOV of ~1 cm. The possible

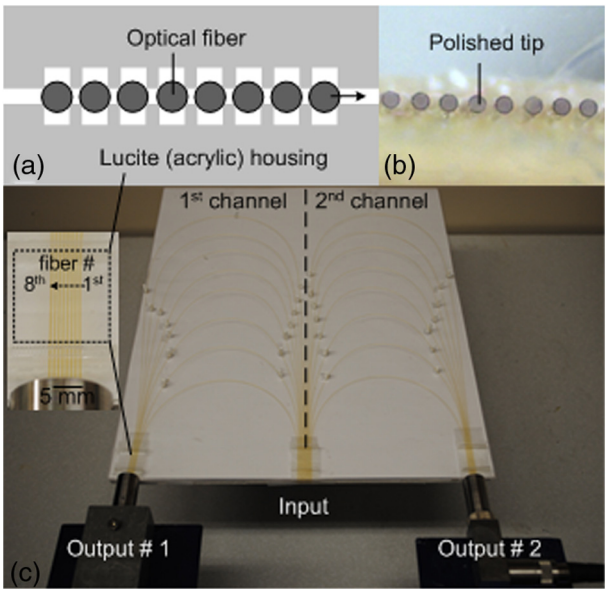

Fig. 5 (a) Schematic of the parallel arrangement of fiber endings in equally spaced trenches. (b) Optical microscopic image showing polished tips of fibers. (c) Picture of the PADL array having a common input and two output channels. Inset shows the picture of equally spaced Lucite grooves housing the fiber endings.

increase in field-of-view due to ultrasound acceptance angle is neglected, since that effect is small compared to the size of the delay line input port which is the dominant factor here.

4 Photoacoustic Imaging with PADLs

4.1 *Photoacoustic Imaging Experiment*

Figure 6 shows the PA experimental setup. The light was delivered from a tunable OPO laser (Surelite OPO PLUS; Continuum; with a wavelength tunability of 410 to 2500 nm) pumped by a Q-switched Nd:YAG laser (SLII-10; Continuum) with a 5-nanosecond pulse duration and a 10-Hz pulse repetition rate. A light wavelength of 800 nm was used. The first two lenses collimated the laser beam, and the cylindrically focused light beam, horizontally parallel to the PADLs, illuminated the sample surface. This obliquely incident dark-field light illumination, which shined above the interface between the delay lines and the tissue phantom, helped reduce the generation of unwanted surface signals at the interface. The incident laser pulse energy was less than 5 mJ/cm^2, far below the ANSI safety limit of 31 mJ/cm^2 at this wavelength.

Generated PA waves were detected by the PADLs, which were divided into two channels. For each channel, eight distinct PA waves propagating via the optical fibers were time-delayed and serially detected by a single-element unfocused ultrasound transducer with a center frequency of 1 MHz (Olympus NDT, V303). The PA signals were amplified and received by an oscilloscope. To enhance the coupling efficiency and minimize unwanted ultrasound reverberation, ultrasound gel was applied at the interfaces between the optical fibers and the ultrasound transducer surface. A standard PAT reconstruction algorithm was employed to reconstruct the PA image, and the Hilbert transformation was taken in the axial direction for envelope detection.[35]

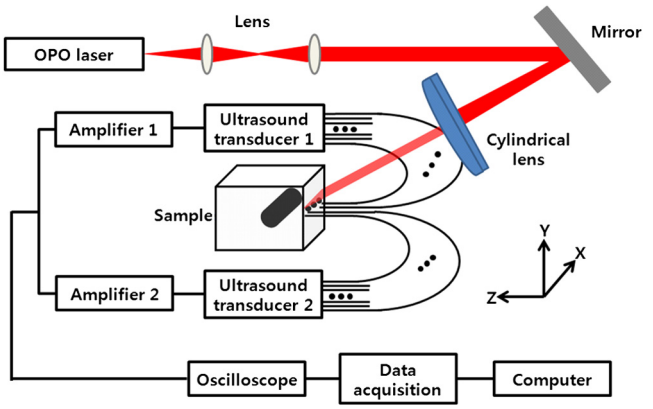

Fig. 6 PA experimental setup using 16 channels of optical-fiber PADLs with two DAQ channels. Each DAQ channel interfaces with 8 optical-fiber PADLs.

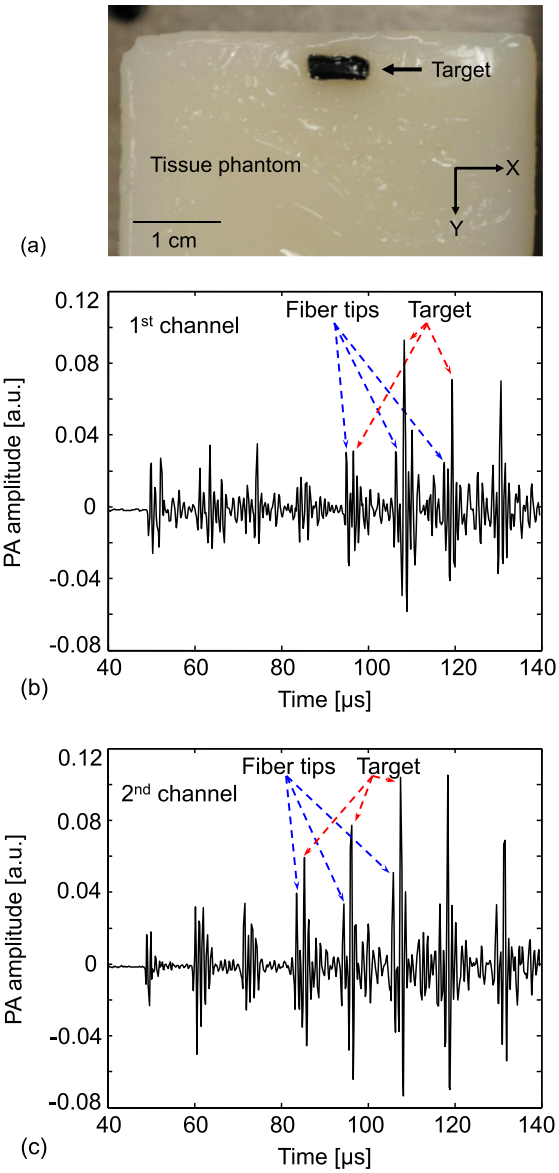

Fig. 7 Reconstructed PA image of an optically absorptive target embedded in an optically scattering medium. (a) Photograph. (b) Raw A-scan data received by the first channel. (c) Raw A-scan data received by the second channel.

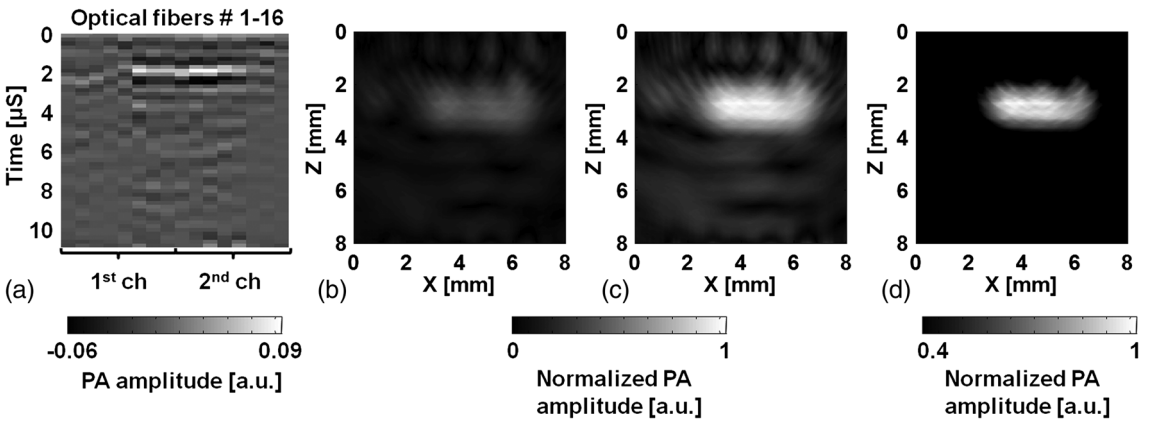

Fig. 8 (a) Reshaped raw data acquired by both channels. Reconstructed PA images (b) without; and (c) with compensation of the acoustic attenuation in each fiber. (d) Thresholded (40%) PA image of (c).

4.2 *Photoacoustic Image*

To investigate the potential for cross-sectional imaging, an optically scattering tissue phantom ($100 \times 100 \times 50$ mm^3 along the x, y, and z axes, respectively) containing an optically absorptive object ($5 \times 2 \times 2$ mm^3 along the x, y, and z axes, respectively) was used [Fig. 7(a)]. The target was positioned at a depth of 3 mm from the sample surface. The phantom was made of 10% gelatin by weight and 1% intra-lipid by volume, and its reduced scattering coefficient was ~9 cm^{-1}. The absorption coefficient of the object was ~100 cm^{-1}. The A-scan PA signals received from the two channels are shown in Fig. 7(b) and 7(c). Each A-scan sequentially recorded PA signals detected by each fiber. In theory, the PA signals from each fiber can be distinguished by calculating the fiber length differences and the acoustic velocity in the fiber. However, even minor measurement errors of these two parameters may cause inaccurate time delays and severely distort the image reconstruction. To address this issue, the starting points of the fibers were directly measured by painting the fiber tips with black ink, which also generated PA signals upon laser illumination. Thus the peaks of the PA signals from the ink on the fiber tips can be treated as the starting points and help indicate the actual PA signals corresponding to the imaged target.

The PA signals were averaged 100 times, so the imaging speed for one PA image was 10 s. A-scans from both ultrasonic transducers were reshaped and combined into one data set, as shown in Fig. 8(a). The reconstructed PA images without and with compensation of the acoustic attenuation (0.2 dB/cm) in each fiber are shown in Fig. 8(b) and 8(c), respectively, which match well with the photograph in Fig. 7(a). The image contrast, defined as the ratio of the difference in PA signals measured from the target and background to that acquired from the background, is estimated to be ~3.0; and the contrast-noise-ratio is 10.8. The spatial resolution, defined as the one-way distance across the 10% and 90% points between the maximum and minimum of the edge spread function, is ~800 μm. The PA image contrast may be further enhanced by using a signal threshold of 40%, as shown in Fig. 8(d).

5 Conclusion

In this work, we have developed parallel-acoustic-delay-line (PADL)-based PAT, where multiple channels of PA signals are time-delayed to reduce the complexity of the ultrasonic receiving systems. To provide the needed time-delay, the performance of silica optical fibers serving as acoustic waveguides was experimentally characterized and a 16-channel PADL array was constructed. The feasibility of PADL-PAT was qualitatively demonstrated by conducting PA imaging of a tissue phantom housing an optically absorptive object. By using the PADLs, only two transducers and two channels of DAQ electronics were needed for the PA imaging. In contrast, a conventional PACT would require a 16-element ultrasonic transducer array and 16 channels of DAQ electronics. In this case, ~90% hardware reduction was achieved with the PADL approach. To fully develop and optimize the PADL-PAT system for preclinical and clinical applications, the following studies need to be performed in the future: 1. the analysis of the coupling efficiency of acoustic waves between the medium and the fiber delay lines; 2. quantitative measurements of PA amplitudes by varying the absorption coefficients of the objects, imaging depths, and laser fluence; 3. the analysis of the response function of each delay line; and 4. development of a hardware system to efficiently isolate the PA echo signals between delay lines.

Once fully developed and optimized, the PADL approach could be applied to enhance the clinical applications of real-time 2D or even three-dimensional (3-D) PA and ultrasound imaging with significantly reduced system cost.

Acknowledgments

This work was supported in part by grants from the National Institutes of Health (R01 EB000712, R01 EB008085, R01 CA134539, U54 CA136398, and R01 CA157277). L. V. Wang has a financial interest in Microphotoacoustics, Inc. and in Endra, Inc., which, however, did not support this work. C. Kim and M. Jeon were supported by the University at Buffalo faculty start-up fund. C.-C. Chang and J. Zou were supported in part by a grant from the National Institutes of Health (U54 CA136398) and a grant from the National Science Foundation (CMMI-1131758).

References

1. A. A. Oraevsky and A. A. Karabutov, "Optoacoustic tomography," Chapter 34 in *Biomedical Photonics Handbook* Vol. PM125, T. Vo-Dinh, Ed., pp. 3401–3434, CRC Press, Boca Raton, FL (2003).
2. C. Kim, C. Favazza, and L. V. Wang, "*In vivo* photoacoustic tomography of chemicals: high-resolution functional and molecular optical imaging at new depths," *Chem. Rev.* **110**(5), 2756–2782 (2010).

3. L. V. Wang, *Photoacoustic Imaging and Spectroscopy*, CRC Press, Boca Raton, FL (2009).
4. M. -L. Li et al.,"Simultaneous molecular and hypoxia imaging of brain tumors *in vivo* using spectroscopic photoacoustic tomography," *Proc. IEEE* **96**(3), 481–489 (2008).
5. T. Wilson and C. Sheppard, *Theory and Practice of Scanning Optical Microscopy*, Academic Press, London (1984).
6. D. A. Sipkins et al., "*In vivo* imaging of specialized bone marrow endothelial microdomains for tumour engraftment," *Nature* **435**(7044), 969–973 (2005).
7. W. Denk, J. H. Strickler, and W. W. Webb, "Two-photon laser scanning fluorescence microscopy," *Science* **248**(4951), 73–76 (1990).
8. P. T. C. So et al., "Two-photon excitation fluorescence microscopy," *Ann. Rev. Biomed. Eng.* **2**(1), 399–429 (2000).
9. Z. Guo, L. Li, and L. V. Wang, "On the speckle-free nature of photoacoustic tomography," *Med. Phys.* **36**(9), 4084–4088 (2009).
10. H. F. Zhang et al., "Functional photoacoustic microscopy for high-resolution and noninvasive *in vivo* imaging," *Nat. Biotechnol.* **24**(7), 848–851 (2006).
11. X. Wang et al., "Non-invasive laser-induced photoacoustic tomography for structural and functional imaging of the brain *in vivo*," *Nat. Biotechnol.* **21**(7), 803–806 (2003).
12. R. I. Siphanto et al., "Serial noninvasive photoacoustic imaging of neovascularization in tumor angiogenesis," *Opt. Express* **13**(1), 89–95 (2005).
13. J. Laufer et al., "Quantitative spatially resolved measurement of tissue chromophore concentrations using photoacoustic spectroscopy: application to the measurement of blood oxygenation and hemoglobin concentration," *Phys. Med. Biol.* **52**(1), 141–168 (2007).
14. S. Yang et al., "Functional imaging of cerebrovascular activities in small animals using high-resolution photoacoustic tomography," *Med. Phys.* **34**(8), 3294–3301 (2007).
15. L. Li et al., "Photoacoustic imaging of lacZ gene expression *in vivo*," *J. Biomed. Opt.* **12**(2), 020504 (2007).
16. A. De La Zerda et al., "Carbon nanotubes as photoacoustic molecular imaging agents in living mice," *Nat. Nanotechnol.* **3**(9), 557–562 (2008).
17. J. A. Copland et al., "Bioconjugated gold nanoparticles as a molecular based contrast agent: implications for imaging of deep tumors using optoacoustic tomography," *Mol. Imaging Biol.* **6**(5), 341–349 (2004).
18. S. Mallidi et al., "Molecular specific optoacoustic imaging with plasmonic nanoparticles," *Opt. Express* **15**(11), 6583–6588 (2007).
19. D. Razansky and V. Ntziachristos, "Hybrid photoacoustic fluorescence molecular tomography using finite element- based inversion," *Med. Phys.* **34**(11), 4293–4301 (2007).
20. C. Kim et al., "*In vivo* molecular photoacoustic tomography of melanomas targeted by bio-conjugated gold nanocages," *ACS Nano* **4**(8), 4559–4564 (2010).
21. L. V. Wang, "Multiscale photoacoustic microscopy and computed tomography," *Nat. Photon.* **3**(9), 503–509 (2009).
22. M. P. Fronheiser et al., "Real-time optoacoustic monitoring and three-dimensional mapping of a human arm vasculature," *J. Biomed. Opt.* **15**(2), 021305 (2010).
23. J. Gamelin et al., "A real-time photoacoustic tomography system for small animals," *Opt. Express* **17**(13), 10489–10498 (2009).
24. L. Song et al., "High-speed dynamic 3-D photoacoustic imaging of sentinel lymph node in a murine model using an ultrasound array," *Med. Phys.* **36**(8), 3724–3729 (2009).
25. C. Kim et al., "Handheld array-based photoacoustic probe for guiding needle biopsy of sentinel lymph nodes," *J. Biomed. Opt.* **15**(4), 046010 (2010).
26. I. L. Auerbach et al., "Mercury delay line memory using a pulse rate of several megacycles," *Proc. IRE* **37**(8), 855–861 (1949).
27. D. L. Arenberg, "Ultrasonic solid delay lines," *J. Acoust. Soc. Am.* **20**(1), 1–26 (1948).
28. J. E. May, "Wire-type dispersive ultrasonic delay lines," *IRE Trans. Ultrason. Eng.* **7**(2), 44–52 (1960).
29. G. D. Boyd, L. A. Coldren, and R. N. Thurston, "Acoustic clad fiber delay lines," *IEEE Trans. Son. Ultrason.* **24**(4), 246–252 (1977).
30. T. Moriya, Z. Hu, and Y. Tanahashi, "Development of flexible acoustic transmission line for intravascular ultrasonography," *IEEE Ultrason. Symp.*, Vol. 2, pp. 1227–1230, IEEE, San Juan (2000).
31. J. S. Palfreeman, "Acoustic delay lines-a survey of types and uses," *Ultrasonics* **3**(1), 1–8 (1965).
32. I. L. Gelles, "Optical fiber ultrasonic delay lines," *J. Acoust. Soc. Am.* **39**(6), 1111–1119 (1966).
33. E. A. Lindgren, M. Rosen, and K. E. Amin, "Ultrasonic characterization of ceramic fibres at ambient and elevated temperatures," *Ultrasonics* **32**(6), 411–419 (1994).
34. *Panametrics Ultrasonics Transducers Data Sheet*, Olympus NDT, Massachusetts (2006).
35. M. Xu and L. V. Wang, "Universal back-projection algorithm for photoacoustic-computed tomography," *Phys. Rev. E* **71**(1), 016706 (2005).